

# Synthesis of DNA-boron cluster composites and assembly into functional nanoparticles with dual, anti-EGFR, and anti-c-MYC oncogene silencing activity

Katarzyna Bednarska-Szczepaniak,<sup>[a]</sup> Katarzyna Ebenryter-Olbińska,<sup>[b]</sup> Gabriela Gajek,<sup>[c]</sup> Krzysztof Śmiałkowski,<sup>[a, e]</sup> Justyna Suwara,<sup>[b]</sup> Lidia Fiedorowicz,<sup>[d, e]</sup> and Zbigniew Leśnikowski<sup>\*[a]</sup>

A versatile method for the automated synthesis of composites containing DNA-oligonucleotides and boron cluster scaffolds and their assembly into functional nanoparticles is described. The obtained, torus-like nanoparticles carry antisense oligonucleotides that target two different oncogenes simultaneously. The nanoparticles exhibited notable silencing efficiency in vitro

in a pancreatic carcinoma cell line PANC-1 toward EGFR and c-Myc genes at the mRNA level, and a significant efficiency at the protein level. The proposed approach may be an attractive alternative to methods currently used, including one therapeutic nucleic acid, one genetic target, or the use of cocktails of therapeutic nucleic acids.

## Introduction

Nearly half a century after Stephenson and Zamecnik proposed the concept of antisense oligonucleotides (ASOs), nucleic acid-based drugs<sup>[1]</sup> are now a focus of clinicians and the pharmaceutical industry. In addition to ASOs, many other types of therapeutic nucleic acids (TNAs) have been developed. These TNAs have demonstrated potential in treating human diseases, such as cancer, viral infections, and genetic disorders, and as vaccines.<sup>[2]</sup>

To date, sixteen oligonucleotide drugs and several COVID-19 vaccines have received regulatory approval from the FDA/EMA.<sup>[2,3]</sup> A characteristic feature of these TNAs is that they are directed against one specific biological target and one specific RNA or DNA sequence. Consequently, TNAs currently used in clinical practice are administered as monotherapy.<sup>[4]</sup>

Although work on the use of TNA combinations has been performed for many years<sup>[5–7]</sup> this technology, based on the use of TNA cocktails of two or more components or their sequential administration, has not yet reached the stage of clinical applications.

Herein, we propose the use of nanoparticles composed of DNA and boron cluster building blocks comprising two different antisense oligonucleotides targeting two different oncogenes as a dual-acting single agent. To the best of our knowledge, no other type of nanoparticles, with or without boron clusters, with a dual mechanism of action has been described so far. Boron clusters were chosen as a scaffold for building blocks due to their rigid, ball-like structure which allows for precise spatial organization of the attached DNA oligonucleotides at the molecular level. Moreover, the use of different boron clusters allows for obtaining building blocks with different topologies, an important feature in the design and construction of functional nanoparticles. As model targets, EGFR<sup>[8]</sup> and cellular myelocytomatosis oncogene (c-Myc)<sup>[9]</sup> were chosen. Both proteins are overexpressed in several high-mortality human cancers, including pancreatic carcinomas, and are proven therapeutic targets.<sup>[10,11]</sup>

Clinical data analysis for numerous cancers based on the Gene Expression Profiling Interactive Analysis (GEPIA) web server of RNA expression data,<sup>[12]</sup> revealed that a high level of mRNA was expressed for both proteins, EGFR and c-Myc, which is associated not only with a low survival rate but also with disease progression in metastatic pancreatic cancer (Figure S31). Therefore, we chose pancreatic cancer as a challenge and cancer type in our studies,<sup>[13]</sup> and the human pancreatic cancer cell line PANC-1 as an in vitro model.<sup>[14,15]</sup>

The described in this communication nanoparticles constitute the second generation of boron cluster-containing DNA nanomaterials. The first generation is nanoparticles made of only one type of building block, EGFR-silencing tripeds containing boron clusters and anti-EGFR antisense

[a] Dr. K. Bednarska-Szczepaniak, K. Śmiałkowski, Prof. Z. Leśnikowski  
Laboratory of Medicinal Chemistry  
Institute of Medical Biology, Polish Academy of Sciences  
Lodowa Łódź, 106, 92-232, Lodz, Poland  
E-mail: zlesnikowski@cbm.pan.pl

[b] Dr. K. Ebenryter-Olbińska, Dr. J. Suwara  
Centre of Molecular and Macromolecular Studies, Polish Academy of Sciences  
Sienkiewicza Łódź, 112, 90-363 Lodz, Poland

[c] Dr. G. Gajek  
Laboratory of Immunobiology of Infections  
Institute of Medical Biology, Polish Academy of Sciences  
Lodowa Łódź, 106, 92-232, Lodz, Poland

[d] L. Fiedorowicz  
Laboratory of Mycobacterium Genetics and Physiology  
Institute of Medical Biology Polish Academy of Sciences  
Lodowa Łódź, 106, 92-232, Lodz, Poland

[e] K. Śmiałkowski, L. Fiedorowicz  
Lodz Institutes of the Polish Academy of Science  
The Bio-Med-Chem Doctoral School, University of Lodz, Poland

Supporting information for this article is available on the WWW under <https://doi.org/10.1002/chem.202303531>

oligonucleotides.<sup>[16,17]</sup> The second generation, dual-action nanoparticles are made of two types of building blocks, one capable of silencing EGFR and the second with an anti-c-Myc antisense oligonucleotide silencing c-MYC (Figure 1A). Silencing expression of both genes in the same cancerous cell should theoretically have a major benefit for inhibiting cancer progression.<sup>[18]</sup> Another type of difference is the use of two different methods for the synthesis of building blocks containing DNA and a boron cluster, which also causes some subtle structural differences between them. It is also important that the new method, described in this work, is much simpler than the first one<sup>[16]</sup> and more convenient.

## Results and Discussion

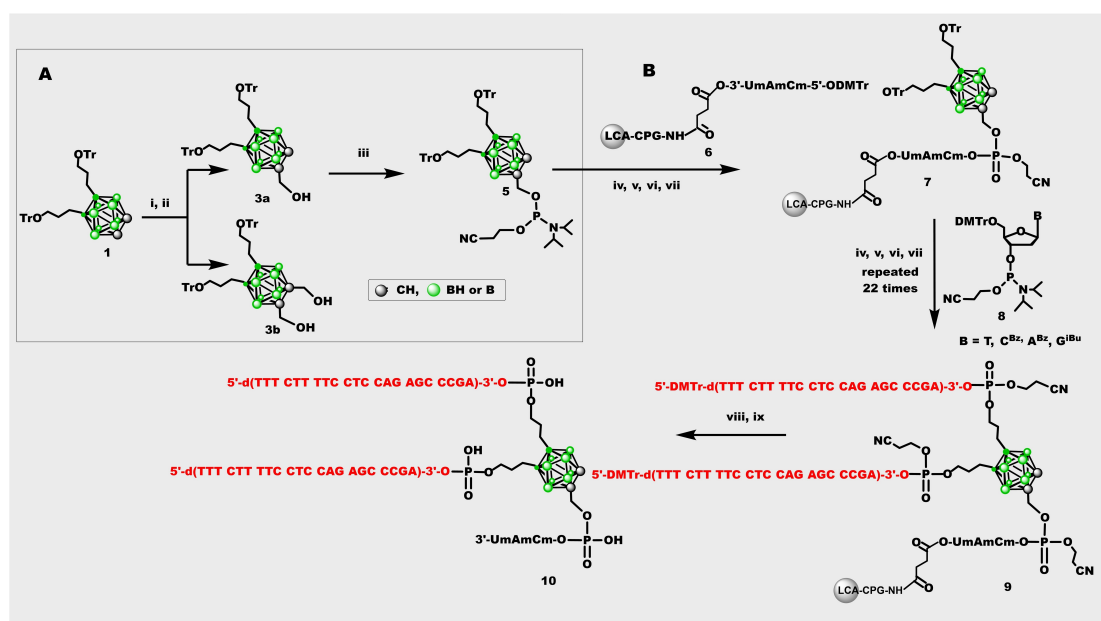
### Automated Synthesis of 1,2-Dicarba-closo-Dodecaborane Triped 10 and 10 thio, and Oligonucleotides 11–14, and 11 thio–14 thio

To construct nanoparticles with dual antisense anti-EGF and anti-c-Myc activity, such as **10** + **11** + **12** (Scheme 1, Figure 1A), two types of building blocks were synthesized. The first one contains derivatives of the 1,2-dicarba-closo-dodecaborane core (Scheme 1) at positions 9 and 12 with 22-mer DNA strands with sequence 5'-d(TTT CTT TTC CTC CAG AGC CCGA)-3',<sup>[18]</sup> complementary (antisense) to the mRNA of the EGFR fragment

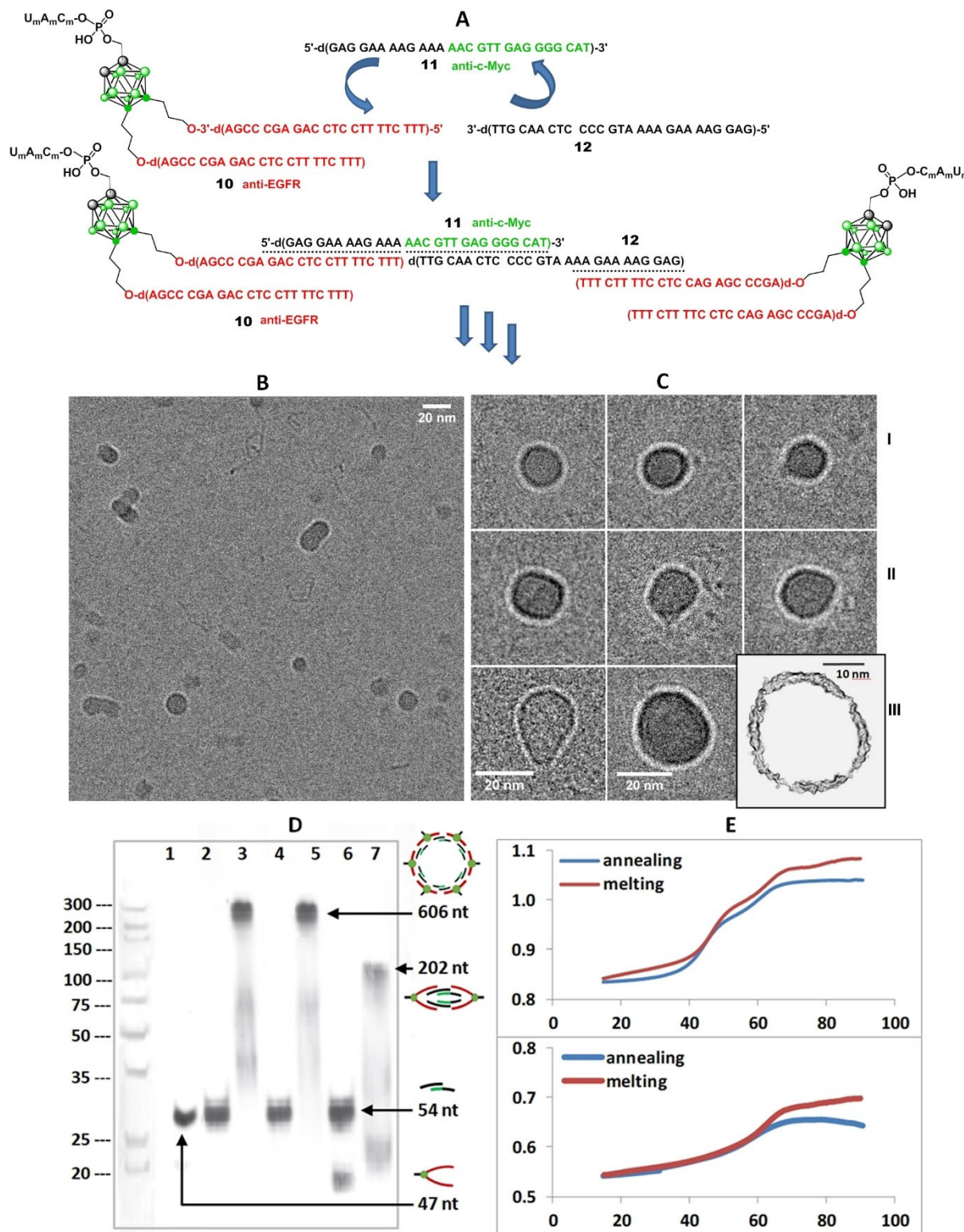
between 51 and 74 nt downstream of the AUG initiation codon,<sup>[19]</sup> and at position 1 of the boron cluster with 3-mer 3'-UmAmCm-5' ("m" means 2'-OMe substituted), providing triped **10** (Scheme 1). The second building block is a DNA duplex linker, such as **11** + **12** composed of strand **11**, which contains an antisense oligonucleotide that targets the first five codons of the c-Myc mRNA<sup>[20]</sup> and a sticky end part complementary to the 5' end of the 22-mer in **10**; and strand **12**, which contains a c-Myc sense fragment and a sticky end part complementary to **10** (Scheme 1, Figure 1A and Table 1). Mixing both types of components leads to the formation of circular and some fraction of linear nanoparticles containing boron clusters and both antisense oligonucleotides, anti-EGFR and anti-c-Myc, due to the formation of duplexes between **10** and linker **11** + **12** (Figure 1).

In the first stage of triped **10** synthesis, an oligofunctionalized boron cluster, 1-(2-hydroxymethyl)-9,12-bis(3-O-tritylprop-1-yl)-1,2-dicarba-closo-undecaborane (**3a**), was obtained,<sup>[16,21, 22]</sup> which was a scaffold, and the antisense, anti-EGFR oligonucleotide were then synthesized thereon (Scheme 1). Under the conditions used, monosubstituted (**3a**) and disubstituted (**3b**) products are formed that can be easily separated by chromatographic methods.

The triped **10** differs from the building blocks described by us earlier<sup>[16]</sup> in two important aspects, the first is the structure and the second is the method of its synthesis. In the first version of **10**,<sup>[16]</sup> in position 1 of the boron cluster is a 2-

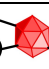
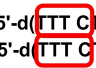

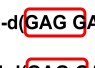
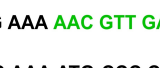
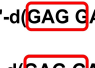
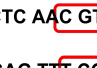
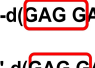
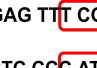
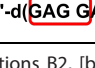
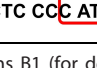


**Scheme 1.** A–Synthesis of 1-(2-hydroxymethyl)-9,12-bis(3-O-tritylprop-1-yl)-1,2-dicarba-closo-dodecaborane (**3a**) and 1-[methyl-O-(N,N-diisopropyl-β-cyanoethyl)phosphoramidite]-9,12-bis(3-O-tritylprop-1-yl)-1,2-dicarba-closo-dodecaborane (**5**). B–Automated, solid phase synthesis of triped **10** containing 1,2-dicarba-closo-dodecaborane 9,12-bis-functionalized with DNA oligonucleotides. A: (i) (CHO)<sub>n</sub> (**2**) in TBAF/THF; (ii) H<sub>2</sub>O; (iii) β-cyanoethyl N,N,N',N'-tetraisopropylphosphordiamidite (**4**), tetrazole in CH<sub>3</sub>CN. B: (iv) detritylation, DMTr/MMTr, 3% DCA in CH<sub>2</sub>Cl<sub>2</sub>; (v) coupling: BMT activator (0.25 M in CH<sub>3</sub>CN); (vi) oxidation: 0.1 M solution of I<sub>2</sub> in THF/H<sub>2</sub>O/pyridine (70:10:20; v/v/v); (vii) capping: 5% phenoxyacetic anhydride in THF/pyridine and 10% solution of 1-methylimidazol/THF/pyridine (1:8:1; v/v/v) for 30 s; (viii) cleavage from the solid support and nucleobase deprotection: 1 mL NH<sub>4</sub>OH (30%) overnight, (ix) detritylation: 2% TFA. A: (i) (CHO)<sub>n</sub> (**2**) in TBAF/THF; (ii) H<sub>2</sub>O; (iii) β-cyanoethyl N,N,N',N'-tetraisopropylphosphordiamidite (**4**), tetrazole in CH<sub>3</sub>CN. B: (iv) detritylation, DMTr/MMTr, 3% DCA in CH<sub>2</sub>Cl<sub>2</sub>; (v) coupling: BMT activator (0.25 M in CH<sub>3</sub>CN); (vi) oxidation: 0.1 M solution of I<sub>2</sub> in THF/H<sub>2</sub>O/pyridine (70:10:20; v/v/v); (vii) capping: 5% phenoxyacetic anhydride in THF/pyridine and 10% solution of 1-methylimidazol/THF/pyridine (1:8:1; v/v/v) for 30 s; (viii) cleavage from the solid support and nucleobase deprotection: 1 mL NH<sub>4</sub>OH (30%) overnight, (ix) detritylation: 2% TFA.



**Figure 1.** A—Schematic representation of the assembly of nanoconstruct **10 + 11 + 12** from tripped **10** and double-stranded linker **11 + 12** with sticky ends 5'-d(GAGGAAAAGAAA...)-3' complementary to the 5'-terminal part of tripped **10**. B and C—cryo-TEM images of complex **10 + 11 + 12** (1:1:1 molar ratio). B—Population of closed structures with a diameter of 12–30 nm; an admixture of linear, unclosed structures is also visible; scale bars of 20 nm are shown on representative images. C—Circular structures composed of 3 (I), 4 (II) and 5–6 (III) **10 + 11 + 12** units. The processed image is shown as an inserted graphic (lower right). D—Nondenaturing PAGE analysis of the self-assembly products of **10** and their partially complementary anti-c-Myc components used in equimolar amounts. On the left—marker; Lane 1—**10**; Lane 2—duplex **11 + 12**; Lane 3—three-component objects **10 + 11 + 12**; Lane 4—duplex **11 thio + 12**; Lane 5—three-component objects **10 thio + 11 thio + 12**; Lane 6—duplex **11 thio + 12 thio**; Lane 7—three-component objects **10 thio + 11 thio + 12 thio**. E—The UV-monitored thermal dissociation and association curves for the nanoconstruct **10 + 11 thio + 12** ( $T_m = 46.5 \pm 0.7^\circ\text{C}$  and  $61.1 \pm 1.1^\circ\text{C}$ ) and double-stranded linker **11 thio + 12** ( $T_m = 59.9 \pm 0.6^\circ\text{C}$ ).

**Table 1.** Sequences of oligonucleotide building blocks: triped **10** and **10thio** targeted against EGFR and components of double-stranded linkers; hybrid oligonucleotide **11** containing anti-sense sequence targeted against c-Myc and sense fragment complementary with 5'-part of anti-EGFR oligonucleotide in **10**, and complementary sequence **12**; antisense oligonucleotide targeted against c-Myc **11thio** and complementary sequence **12thio**; and control oligonucleotides containing scramble sequences, **13**, **14** and **13thio**, **14thio**.

No.	Oligonucleotide sequence	m/z calc.	m/z MS	Rt [min]	UV [nm]
<b>10</b>	5'-d(TTT CTT TTC CTC CAG AGC CCGA)-  -CmAmUm-3'	14623.2	13628.3 <sup>[c]</sup>	11.6 <sup>[a]</sup>	265
<b>10thio</b>	5'-d(  TTT CTT TTC CTC CAG AGC CCGA)-  -CmAmUm-3'	14715.7	13757.5 <sup>[c]</sup>	12.1 <sup>[a]</sup>	265
<b>11</b>	5'-d(GAG GAA AAG AAA AAC GTT GAG GGG CAT)-3'	8479.6	8478.5	12.4 <sup>[b]</sup>	255
<b>12</b>	5'-d(GAG GAA AAG AAA ATG CCC CTC AAC GTT)-3'	8310.5	8309.4	12.7 <sup>[b]</sup>	257
<b>13</b>	5'-d(GAG GAA AAG AAA CAT GGG GAG TTT CGA)-3'	8470.6	8469.4	12.1 <sup>[b]</sup>	257
<b>14</b>	5'-d(GAG GAA AAG AAA TCG AAA CTC CCC ATG)-3'	8319.5	8319.9	12.7 <sup>[b]</sup>	257
<b>11thio</b>	5'-d(  GAG GAA AAG AAA  AAC GTT GAG GGG CAT)-3'	8575.6	8576.4	13.1 <sup>[b]</sup>	255.4
<b>12thio</b>	5'-d(  GAG GAA AAG AAA ATG CCC CTC  AAC GTT)-3'	8406.5	8406.3	13.3 <sup>[b]</sup>	256
<b>13thio</b>	5'-d(  GAG GAA AAG AAA CAT GGG GAG  TTT CGA)-3'	8566.6	8566.3	13.6 <sup>[b]</sup>	257
<b>14thio</b>	5'-d(  GAG GAA AAG AAA TCG AAA CTC  CCC ATG)-3'	8415.5	8415.3	13.3 <sup>[b]</sup>	258

[a] HPLC gradient Conditions B2, [b] HPLC gradient Conditions B1 (for details, please see SI section). **10** and **10thio**, boron cluster core loaded with two identical anti-EGFR 22-mers. [c] The m/z value corresponds to the fragmentation ion without the UmAmCm trinucleotide at boron 2. The zoomed part of the region of the spectrum in the mass range corresponding to the low-intensity molecular ion is shown as an insert in the mass spectra of triped **10** and **10thio** available in SI. 5'-terminal tetranucleotide in **10thio** containing three phosphorothioate groups is marked with a red frame. The hybrid of anti-c-Myc oligonucleotide **11**, nucleosides 13–28 from the 5'-end marked in green, and of sense, sticky fragment (nucleosides 1–12 from the 5'-end) complementary with the 5'-part of the anti-EGFR oligonucleotide in **10**. Hybrid oligonucleotide **12**, complementary to **11** within the anti-c-MYC sequence and to part of the **10** sequence at the 5'-end. **11thio** and **12thio**, counterparts of **11** and **12** protected at the 3'- and 5'-ends with tetranucleotides containing three phosphorothioate groups marked with a red frame. The hybrid of scramble oligonucleotide **13** within the anti-c-Myc part, nucleosides 13–28, and of sense, sticky fragment (nucleosides 1–12 from 5'-end) complementary with 5'-part of anti-EGFR oligonucleotide in **10**. Hybrid oligonucleotide **14** complementary to **13** within the scramble sequence and to part of the **10** sequence at the 5'-end. **13thio** and **14thio** counterparts of **13** and **14** protected at the 3'- and 5'-end with tetranucleotides containing three phosphorothioate groups marked with a red frame.

hydroxyethyl group, while in the new version, in position 1 is a 3-mer tail composed of 2'OMe nucleosides Um, Am, and Cm. This seemingly trivial difference is due to a completely different technique for synthesizing composites of boron clusters and DNA used in this work. In the original method, the LCA-CPG solid support was first prepared with the attached boron cluster,<sup>[16,23]</sup> which was a tedious and time-consuming procedure, and the appropriate DNA oligomers were then synthesized on the boron cluster. In the present method, only the appropriate boron cluster phosphoramidite must be synthesized, such as **5**, and is then attached to a previously synthesized on LCA-CPG support short or longer DNA oligomer. Then, the appropriate DNA oligomers on the boron cluster are synthesized, as shown in Scheme 1.

The advantage of the new method is the use at each stage of the phosphoramidite chemistry and the automatic method of DNA synthesis that is commonly used.<sup>[24,25]</sup>

The second building block is a DNA duplex linker, such as **11** + **12** (Figure 1A and Table 1). The antisense anti-c-Myc part in **11** is the 15-mer sequence 5'-d(AAC GTT GAG GGG CAT)-3' described in the literature.<sup>[20]</sup> Another oligodeoxynucleotide used was oligonucleotide **13**, a counterpart of **11** with a scramble 15-mer sequence within the c-Myc part of **11** complementary to oligonucleotide **14**, used to build a control

double-stranded linker **13** + **14** (Table 1).<sup>[26]</sup> Nucleolytic degradation of therapeutic nucleic acids in biological environments is a problem that necessitates constant attention for practical ASO applications. Hence, in clinical practice, phosphorothioate analogs of ASOs that contain some or all phosphorothioate bonds in the oligonucleotide backbone instead of the natural internucleotide linkages are often used.<sup>[2,27]</sup> Therefore, all oligonucleotide derivatives used in our research (Table 1) were obtained not only in the basic version containing natural phosphodiester internucleotide linkages but also as derivatives **10thio** and **11thio**–**14thio**, which contain three phosphorothioate internucleotide linkages at the 5' and 3' ends (Table 1) (details of synthesis in SI). Due to the favorable physicochemical properties, sufficient thermodynamic stability of the formed nanoconstructs, and resistance to nucleolytic degradation (vide infra), **10** + **11thio** + **12** was used in the silencing experiments with the target genes of EGFR and c-Myc.

### Self-assembly of tripeds and components of the double-stranded linker into nanoconstructs 10 + 11 + 12, 10 + 13 + 14, 10 + 11 thio + 12, and 10 thio + 11 thio + 12 thio

The nanoconstructs were formed by annealing a mixture of tripod **10** or **10 thio** and components of DNA duplex linkers, such as **11**, **11 thio**, or **13**, and complementary strands **12**, **12 thio**, or **14** in a 1:1:1 molar ratio (detailed procedure in SI). Notably, when simply mixing components **10**, **11**, **12**, or **10**, **11 thio**, **12** at ambient temperature, an identical population of **10 + 11 + 12** or **10 + 11 thio + 12** nanoconstructs is formed, as observed when the mixture of components is heated and cooled (Figure 1A), which may be of practical importance and facilitate the use of nanoconstructs in practice. Through electrophoretic analysis, the assembled structures formed by tripeds **10** or **10 thio** and single-stranded oligonucleotide components **11–14** and **11 thio–12 thio** could be visualized.

Autoradiographic analysis reveals one dominant product accounting for approximately 300-base pair (606 nt) DNA constructs, which can correspond to circular complexes formed of a total of 6 tripeds **10** and 6 double-stranded linkers **11 + 12** as estimated in comparison to the dsDNA size marker. More precise sizes of the nanoobjects can be accessed from the cryo-TEM studies discussed below.

It should be emphasized that despite the clear tendency to form nanostructures of similar size, the pool of emerging objects is not fully homogeneous, and objects of various sizes are visible in the form of smears on PAGE gels (Figure 1D and Figure S33 and S34) and cryo-TEM images (Figure 1B).

The impact of the chemical modification of the components with phosphorothioate groups on the efficiency of the nanoconstruct assembly was also studied. It was found that the introduction of three phosphorothioate groups at both the 3'- and 5'- ends of one strand of a double-stranded linker, as in **11 thio + 12**, does not affect the ability to form nanoconstructs (Figure 1D). However, a different situation was observed when all components of the nanoconstruct: **10 thio**, **11 thio** and **12 thio** were protected with phosphorothioate internucleotide linkages at the ends of DNA-oligomers. In this case, the destabilizing effect of phosphorothioate groups, which are a mixture of P-diastereomers, on the stability of the duplexes formed prevents the formation of molecular structures higher than approximately 200 nt (Figure 1D).

It therefore seems that the destabilizing effect of phosphorothioate groups with undefined absolute configurations at the phosphorus atom, which is ignored in the case of phosphorothioate ASO drugs, is significant in the case of the self-assembly of DNA nanoconstructs. This phenomenon is discussed in more detail below in the section describing the thermodynamic properties of nanoconstructs.

### Cryogenic transmission electron microscopy (cryo-TEM)

Samples for the cryo-TEM measurement were prepared in the same manner as for the physicochemical and biological studies, as described in the Materials and Methods section in SI. The

collected cryo-TEM measurement data were transferred to .mrc files, compressed, and subjected to lossless processing into images in .tiff format. Then, to visualize the structures, the images were subjected to contrast and smoothing (Figure 1B and 1 C).

Selected objects were analyzed individually, background noise was reduced and, using the denoising and finding edges functions, the contours of the structures were found (Figure 1C, inserted graphic). Structures were sized using ImageJ 1.54 tools.

For complex **10 + 11 + 12** used in this study, regular ring nanostructures are formed with various diameters ranging from 12 to 30 nm, which roughly corresponds to structures built of units **10 + 11 + 12** from 2 to 6 (Figure 1C), consisting of tripiped **10** and double-stranded linker **11 + 12**. Small amounts of linear, unclosed structures of varying lengths are also observed (Figure 1B).

### Thermodynamic studies of nanoconstructs and their components

The appropriate nanoconstructs were subjected to UV-monitored thermal melting experiments. Nanoconstruct **10 + 11 thio + 12**, which was used as a dual-action silencing agent in biological experiments, and nanoconstructs **10 + 11 + 12**, **10 thio + 11 thio + 12 thio** as well as double-stranded linkers **11 thio + 12**, **11 + 12** and **11 thio + 12 thio** used for comparison, were tested. The thermodynamic parameters of the association/dissociation process were calculated with the MeltWin program.<sup>[28]</sup> The selected thermodynamic data for the melting transitions and the respective melting temperatures for all tested duplexes are shown in Table 2, and full data are shown in Table S2. The graphical presentation of the **10 + 11 thio + 12** nanoconstruct and double-stranded linker **11 thio + 12** performance is presented in Figure 1E.

**Table 2.** Thermodynamic parameters and melting temperatures of the double strand to single strand duplex transitions for nanoconstruct **10 + 11 thio + 12** and of other structures tested for comparison.

Oligonucleotide	$\Delta G$ [kcal/mol]	$T_m$ [°C] <sup>[a]</sup>	$T_m$ [°C] <sup>[b]</sup>
<b>10 + 11</b>	$-9.6 \pm 0.0$	$48.1 \pm 0.3$	$50.8 \pm 0.2$
<b>10 + 12</b>	$-9.6 \pm 0.0$	$48.1 \pm 0.3$	$64.4 \pm 0.3$
<b>11 + 12</b>	$-16.6 \pm 0.4$	$63.8 \pm 0.6$	$62.9 \pm 0.4$
<b>10 + 12</b>	$-9.5 \pm 0.2$	$41.1 \pm 0.5$	$42.6 \pm 0.8$
<b>10 + 11 thio</b>	$-9.8 \pm 0.1$	$46.6 \pm 0.8$	$46.6 \pm 0.8$
<b>10 + 12</b>	$-9.8 \pm 0.1$	$47.7 \pm 0.6$	$61.2 \pm 1.2$
<b>11 thio + 12</b>	$-14.6 \pm 0.6$	$60.6 \pm 0.7$	$59.9 \pm 0.6$
<b>10 thio + 11 thio</b>	$-9.0 \pm 0.3$	$42.2 \pm 3.5$	$47.6 \pm 1.6$
<b>10 thio + 12 thio</b>	$-9.0 \pm 0.3$	$42.3 \pm 3.5$	$60.4 \pm 0.2$
<b>11 thio + 12 thio</b>	$-13.2 \pm 0.6$	$59.1 \pm 0.8$	$58.4 \pm 1.0$

[a] Thermodynamic parameters ( $T_m$  free Gibbs energy  $\Delta G^\circ$ ; enthalpy  $\Delta H^\circ$  and entropy  $\Delta S^\circ$ ; please see Table S2). [b] The melting temperatures were calculated using the first derivative method (for the two-component system) or second derivative for ternary models.

As expected, simple, two-component linkers containing three phosphorothioate internucleotide linkages at the 5' and 3' ends within one (**11 thio**+**12**) or both (**11 thio**+**12 thio**) complementary strands show lower  $T_m$  values than the corresponding linker without phosphorothioate modification **11**+**12**, indicating their lower stability:  $T_m$  **11**+**12** ( $62.9 \pm 0.4^\circ\text{C}$ ) >  $T_m$  **11 thio**+**12** ( $59.9 \pm 0.6^\circ\text{C}$ ) >  $T_m$  **11 thio**+**12 thio** ( $58.4 \pm 0.9^\circ\text{C}$ ). The melting profiles of three-component systems containing triped **10** (or **10 thio**) with a boron cluster as a core and double-stranded linker show two distinct points of inflection illustrating the biphasic character of the dissociation/association process of the nanoconstructs. An example of the melting curve for the nano-construct **10**+**11 thio**+**12** is shown in Figure 1E, which is also provided for comparison of its double-stranded linker **11 thio**+**12**. The melting curves for the other variants of the nanoconstructs, **10**+**11**+**12** and **10 thio**+**11 thio**+**12 thio**, are shown in Figure S36 in the SI. Comparing the  $T_m$  of the double-stranded linker **11 thio**+**12** ( $59.9 \pm 0.6^\circ\text{C}$ ) and the  $T_m$  of the duplex **10**+**12** formed by triped **10** and oligonucleotide **12**, which is part of the linker **11 thio**+**12**, ( $42.5 \pm 0.7^\circ\text{C}$ ) and the  $T_m$  of the biphasic dissociation of triped **10**+**11 thio**+**12** ( $46.5 \pm 0.7^\circ\text{C}$  and  $61.1 \pm 1.1^\circ\text{C}$ ) (Table 2) allows us to propose the most likely nanoconstruct dissociation scheme. Thus, in the first stage, the double-stranded linker from triped **10** bearing the anti-EGFR antisense sequence was detached and then the double-stranded linker dissociated, leading to the release of the second active antisense oligonucleotide anti-c-Myc **11 thio**.<sup>[29,30]</sup>

The trend observed for the destabilizing effect of the phosphorothioate groups on the stability of nanoconstructs measured by  $T_m$  value was similar to that on double-stranded linkers, although it was less pronounced:  $T_m$  **10**+**11**+**12** ( $50.8 \pm 0.2^\circ\text{C}$  and  $64.3 \pm 0.3^\circ\text{C}$ ) >  $T_m$  **10**+**11 thio**+**12** ( $46.5 \pm 0.7^\circ\text{C}$  and  $61.1 \pm 1.1^\circ\text{C}$ )  $\cong$   $T_m$  **10 thio**+**11 thio**+**12 thio** ( $47.6 \pm 1.6^\circ\text{C}$  and  $60.3 \pm 0.2^\circ\text{C}$ ).

Particular attention should be focused on the observed decrease in the stability of nanoconstructs, as measured by  $T_m$  after phosphorothioate groups (PS) are introduced.<sup>[31]</sup> Replacing the achiral phosphodiester internucleotide linkage with a chiral phosphorothioate diester center that exhibits two distinct stereochemical configurations (designated  $S_p$  and  $R_p$ ) can have a profound effect on the properties of modified TNAs.<sup>[32]</sup>

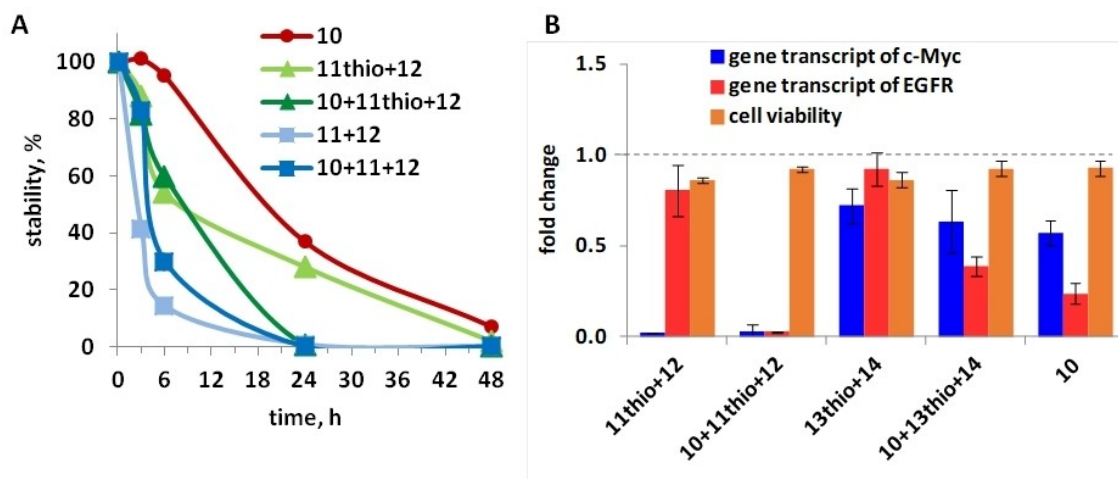
Research on stereocontrolled chemical methods of internucleotide linkage formation in the synthesis of modified DNA/RNA has been conducted for a long time,<sup>[32–34]</sup> but no practical and scalable methods have been reported thus far. As a result, mixtures of up to  $2^n$  individual drug molecules (diastereoisomers of TNAs) differing in properties, in which  $n$  equals the number of chiral, internucleotide phosphorothioate linkages, are used in clinical practice as a compromise.<sup>[35]</sup> However, our observations indicate that this compromise may be acceptable at the present stage of method development for the stereospecific synthesis of phosphorothioate modifications of nucleic acid drugs, but it is less acceptable when these mixtures are used as building blocks in nanoconstruction for chemotherapeutic or other applications. This is evidenced by the decrease in  $T_m$  of nanoconstructs **10 thio**+**11 thio**+**12 thio** in compar-

ison to **10**+**11**+**12** or **10**+**11 thio**+**12** and the inability of **10 thio**+**11 thio**+**12 thio** to create nanoconstructs with a higher molecular weight, as shown by PAGE studies (Figure 1D, Lane 7).

These results prompted us to use in gene silencing experiments the dual-action nanoconstruct **10**+**11 thio**+**12** that contains only one crucial component, **11 thio**, which is protected by phosphorothioate modifications. Based on the increased resistance of triped **10** to nucleolytic degradation due to the presence of the boron cluster modification observed earlier,<sup>[37]</sup> protecting the triped with phosphorothioate modifications was abandoned.

#### Serum stability of nanoconstructs **10**+**11 thio**+**12** and **10**+**11**+**12**, corresponding to double-stranded linkers **11 thio**+**12** and **11**+**12** and single-stranded components **10**, **11**, and **11 thio**

To test the stability of the nanoconstructs used in silencing experiments and their components in biological environments, experiments using human serum were performed. Human serum contains several exo- and endonucleolytic activities that are responsible for the digestion of unmodified and phosphorothioate-modified oligonucleotides.<sup>[36]</sup> We compared the stability of nanoconstruct **10**+**11**+**12**, which contains unprotected oligonucleotide components, and nanoconstruct **10**+**11 thio**+**12**, which contains anti-c-Myc antisense oligonucleotide **11** and **11 thio** protected with three phosphorothioate linkages at the 3' and 5' termini. The stability of protected and unprotected oligonucleotide building blocks **10** and **11**+**12** was also tested (for experimental details please see the SI section). The most stable form contained boron cluster modification triped **10** with  $t_{1/2} = 19.5$  h and chimeric duplex **11 thio**+**12** with  $t_{1/2} = 10.0$  h bearing **11 thio** protected with three phosphorothioate internucleotide linkages at both 3' and 5' ends and unprotected, complementary strand **12**. The nanoconstruct **10**+**11 thio**+**12** was less stable overall with  $t_{1/2} = 7.6$  h. It should be remembered, however, that in the case of **10**+**11 thio**+**12** or **10**+**11**+**12**, the decrease in the concentration of the intact nanoconstruct is affected not only by enzymatic degradation but also, probably to a greater extent, by dissociation into the constituent parts containing the anti-EGFR antisense sequence **10** and the **11 thio**+**12** duplex containing the anti-c-Myc oligonucleotide **11 thio**. In this context, the slow dissociation of the nanoconstruct releasing active antisense oligonucleotides and the above-mentioned relatively high resistance to degradation of components **10** and **11 thio**+**12** is highly desirable. Unprotected nanoconstruct **10**+**11**+**12** was degraded faster, with a half-life  $t_{1/2} = 4.9$  h, but remained more stable than **11**+**12** with  $t_{1/2} = 2.3$  h, which became completely digested after 24 hours; only 14% remained after 6 hours (compared to the 30% stability of **10**+**11**+**12** and 60% stability of **11 thio**+**12**, Figure 2A). In addition to the protective function of phosphorothioate internucleotide linkages, the mentioned above possible effect of modification with a boron cluster on the increase in nucleolytic stability cannot be overlooked.<sup>[37]</sup>



**Figure 2.** A—Stability of modified nanostructures with phosphorothioate (thio) internucleotide linkages (11 thio + 12, 10 + 11 thio + 12) in comparison to unmodified components (10, 11 + 12, 10 + 11 + 12) in human serum (experimental details are described in the SI section). B—Viability of PANC-1 cells (orange bars) and silencing of EGFR and c-Myc mRNA transcripts (red and blue bars) in the presence of nanoconstruct 10 + 11 thio + 12, its components 10 and 11 thio + 12 used for comparison, and 10 + 13 thio + 14 and 13 thio + 14 containing scramble sequence in 13 thio + 14 within the anti-c-Myc part of double-stranded module 11 thio + 12, used as negative control for c-Myc (100 nM, 24 h; experimental details are described in the “Reverse transfection” part in SI section).

### Cytotoxicity of nanoconstruct 10 + 11 thio + 12, double-stranded linker 11 thio + 12, and controls

PANC-1 cells were treated with nanoconstructs 10 + 11 thio + 12 or a control 10 + 13 thio + 14 consisting of a scramble sequence instead of the anti-c-Myc sequence in the double-stranded linker. To determine the cytotoxicity of the constructs, an MTT viability assay was performed.

The cytotoxicities of the nanoconstruct components, triped 10 and double-stranded linkers 11 thio + 12 and 13 thio + 14, were also tested. All samples were tested for 24 h at a concentration of 100 nM, which was selected as optimal based on previous studies involving a nanoconstruct build of 10 and complementary triped that were directed against EGFR mRNA.<sup>[16]</sup> Lipofectamine 3000 was used as the transfection reagent, which was not cytotoxic to cells (Figure S32). The MTT results indicate that the screened oligonucleotides are generally nontoxic to the cancer cells, and the mitochondrial activity is only slightly lowered under the conditions used (Figure 2B).

### Silencing of human EGFR and c-MYC mRNA transcripts in PANC-1 cells line exposed to nanoconstruct 10 + 11 thio + 12. Real-time quantitative PCR assay

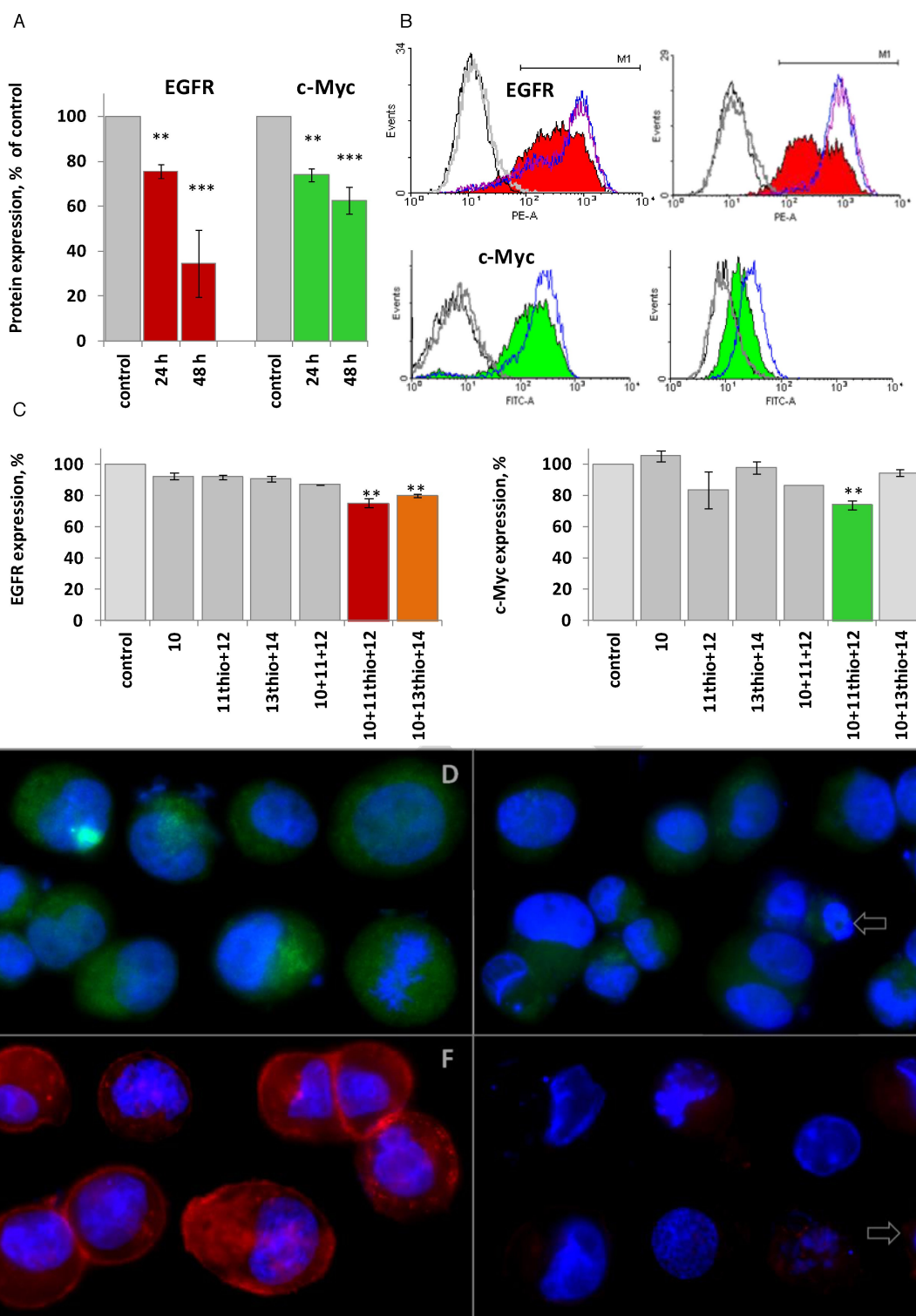
The procedure was performed analogously as described earlier<sup>[38,39]</sup> and in detail in the SI section. A prominent and specific effect of the nanoconstruct 10 + 11 thio + 12 used at 100 nM on the abundance of the EGFR and c-Myc gene-specific transcripts was observed after 24 h, in which both gene transcripts were silenced (Figure 2B)

The specificity of the observed silencing activities is confirmed by the fact that the nanoconstruct 10 + 13 thio + 14 and double-stranded linker 13 thio + 14 that contain the

scramble sequence instead of the anti-c-Myc sequence showed no activity against the c-Myc gene. Triped 10 which contained an antisense sequence targeted against EGFR also exhibited silencing activity, but to a lesser extent than a full nanoconstruct. It also showed small, unspecific activity toward c-Myc transcription. Sequence-nonspecific effects of antisense oligonucleotides are well recognized. This results from the limited requirement of RNase H for long double-stranded substrates. This enzyme is highly specific regarding the type of its substrate's backbone, which must be mRNA/DNA-oligonucleotide heteroduplex; however, RNase H does not require full-length homology between the target mRNA and the incoming antisense oligonucleotide to recognize and cleave the mRNA strand.<sup>[3]</sup> The presence of a centrally located boron cluster in 10 may increase its small, nonspecific activity. This hypothesis is supported by the increase in RNase H activity toward poly r(A) achieved by a short oligothymidylic acid containing boron cluster modification in the central part of the oligomer.<sup>[37]</sup> One possible explanation of this phenomenon may involve the affinity of boron clusters toward both nucleic acids and proteins, which may result in transient “gluing” of the oligonucleotide substrate and the enzyme protein, facilitating mRNA cleavage.<sup>[40,41]</sup>

### Dual silencing of EGFR and c-MYC genes by nano-construct 10 + 11 thio + 12 in PANC-1 cells line. Intra-cellular protein staining

To evaluate the effect of the 10 + 11 thio + 12 construct on c-Myc and EGFR protein levels in PANC-1 cells, an intracellular labeling technique and cytometric measurements, as well as an immunochemical staining method and fluorescence microscopy, were used as described in detail in the SI section. The



**Figure 3.** A—Expression of EGFR and c-Myc proteins in PANC-1 cells incubated with the 10 + 11 thio + 12 (100 nM) for 24 and 48 h, percentage of control cells; mean  $\pm$  SD, 3–6 repeats; \*\* $p < 0.01$ , \*\*\* $p < 0.001$  (Bonferroni test). B—Representative histograms of EGFR and c-Myc protein expression in cells. Blue line histograms—control cells, color-filled—cells with the nanoconstruct, gray line - binding of nonspecific antibodies, black line—background fluorescence of non-stained cells. C—EGFR and c-MYC protein expression in cells treated 10 + 11 thio + 12, 10 + 11 + 12, 10 + 13 thio + 14, 10, 11 thio + 12, or 13 thio + 14 (100 nM, 24 h); mean  $\pm$  SD, 4–6 repeats; \* $p < 0.05$ , \*\* $p < 0.01$  (Bonferroni test). D–G—Epifluorescence microscopy images of PANC-1 cells stained for intracellular visualization of c-Myc (green, D and E), EGFR (red, F and G), and for nuclei (blue, D–G); details are described in Materials and Methods in the SI. D and F—untreated cells, E and G—10 + 11 thio + 12-treated cells (100 nM, 48 h) 1000 $\times$ magnification. Apoptotic nuclei are marked with an arrow (E and G).

activity of the 10 + 11 thio + 12 construct (100 nM) was assessed after 24 h and 48 h and compared to the activity of the

reference scramble 10 + 13 thio + 14 construct. The activity was also compared to other control samples, such as triped 10,



double-stranded linkers **11 thio** + **12** and **13 thio** + **14** and nanoconstruct **10** + **11** + **12**, without phosphorothioate protection of anti-c-Myc sequence **11**. After 24 h of incubation with cells, the **10** + **11 thio** + **12** construct reduced the levels of c-Myc and EGFR proteins by approximately 30% (Figure 2A and Figure 3C). The reference construct containing the scramble sequence instead of the anti-c-Myc sequence (**10** + **13 thio** + **14**) did not affect c-Myc expression as expected and reduced the level of EGFR protein by approximately 20% due to the anti-EGFR activity of **10** present within the structure of the nanoconstruct (Figure 3C). Triped **10** only slightly downregulated EGFR protein expression (Figure 3C). This demonstrates triped **10** more effectively reduces the expression of the EGFR protein when used as a part of nanostructures **10** + **11 thio** + **12** or **10** + **13 thio** + **14**. The nanoconstruct **10** + **11** + **12**, without phosphorothioate protection of anti-c-Myc sequence **11**, reduced the c-Myc protein level less efficiently than the nanoconstruct containing phosphorothioate-protected **11 thio** (Figure 3C). Prolonged incubation of cells with the **10** + **11 thio** + **12** construct (up to 48 h) resulted in a higher decrease in EGFR and c-Myc protein levels, EGFR (by up to 70%) and c-Myc (by 40%) (Figure 3A and 3B).

The c-Myc protein (stained green, Figure 3D and 3E), localized inside the cells, and EGFR (stained red, Figure 3F and 3G) in the cellular membrane were visualized with immunofluorescent images. Cells incubated with the dual anti-sense anti-EGFR and anti-c-MYC **10** + **11 thio** + **12** nano-construct after 48 h of treatment (Figure 3E and 3G) showed a marked decrease in the intensity of green (c-Myc) and red (EGFR) fluorescence. Moreover, as shown in the SI (Figure S35), a decrease in c-Myc- and EGFR-derived fluorescence in the cells was noted after 24 h incubation with the nanoconstruct (Figure S35). Characteristic apoptotic nuclei with chromatin condensation were visible in treated cells (Figure 3E and 3G, and Figure S35B and S35D).

## Conclusions

A second generation of nanoconstructs composed of DNA and boron clusters, which contain two different antisense oligonucleotides that target two different oncogenes as a single, dual-action agent, was described. The pancreatic carcinoma and PANC-1 cell lines were selected as biological models, and the EGFR and c-Myc proteins were selected as biological targets for this study. The nanoparticles used to silence the biosynthesis of EGFR and c-Myc at the mRNA level were demonstrated to be highly efficient by the RT-PCR method, and a significant reduction in both protein levels in cells was observed by the intracellular protein staining method. The proposed dual-action nanoparticle approach may be an attractive alternative to the current monotherapy strategies, including one therapeutic nucleic acid, one genetic target, or the developmental use of cocktails containing different therapeutic nucleic acids. Contrary to these strategies, the strategy proposed in this work is a case of multidrug therapy, consisting of the simultaneous action of two different therapeutic nucleic acids on two different bio-

logical targets, in the same cell. Moreover, its uniqueness is related to the fact that both drugs are administered as one nanoparticle containing both therapeutic components. In addition, in the proposed strategy, dual-action nanoparticles are easily adapted to carry antisense oligonucleotides directed against other target genes, and the nanoparticles are easily optimized.

## Supporting Information

Full experimental details, materials, methods, procedures and full characterization of all compounds, RP-HPLC traces, ESI-MS and <sup>1</sup>H-, <sup>11</sup>B-, <sup>31</sup>P-NMR, FT-IR spectra, survival analysis for pancreatic adenocarcinoma patients for c-Myc and EGFR, PANC-1 cell viability in the presence of nanoconstructs at concentrations of 100 nM and 200 nM, table with full thermodynamic parameters for nanoconstructs and their components, additional PAGE gels.

The authors have cited additional references within the Supporting Information.<sup>[42–46]</sup>

## Acknowledgements

The authors thank Prof. M. Cedzyński and Prof. A. Świerzko for access to the cell culture infrastructure and the gift of pooled human serum, Dr. Michał Rawski for assistance with cryo-TEM measurements. Ms. Dorota Borowiecka and Ms. Agata Kraj of the National Library of Chemical Compounds (NLCC) POL-OPENSOURCE for recording the mass spectra and Dr. Ewelina Wielgus of the Center of Molecular and Macromolecular Studies PAS for recording and refining the mass spectra of compounds **10** and **10 thio**. Funding by National Science Centre in Poland, grant No. 015/16/W/ST5/00413. The electrospray ionization (ESI) mass spectra for low molecular weight compounds 1–5 were recorded on Agilent 6546 LC/Q-TOF at the NLCC established within the project POL-OPENSOURCE financed by the Ministry of Science and Higher Education (decision no. DIR/WK/2018/06 of October 24, 2018). Purchase of the Bruker Avance NEO 400 NMR spectrometer used for <sup>31</sup>P-NMR measurements was supported by the funds from the EU Regional Operational Program of the Lodz Region, RPLD.01.01.00-10-0008/18.).

## Conflict of Interests

The authors declare no conflict of interest.

## Data Availability Statement

The data that support the findings of this study are available from the corresponding author upon reasonable request.

**Keywords:** therapeutic nucleic acids · antisense oligonucleotides · EGFR and c-MYC oncogenes · anti-cancer therapy · boron cluster · nanoparticles

- [1] M. L. Stephenson, P. C. Zamecnik, *Proc. Natl. Acad. Sci. USA* **1978**, *75*, 285–288.
- [2] J. A. Kulkarni, D. Witzigmann, S. B. Thomson, S. Chen, B. R. Leavitt, R. Pieter, P. R. Cullis, R. van der Meel, *Nat. Nanotechnol.* **2021**, *16*, 630–643.
- [3] M. Egli, M. Manoharan, *Nucleic Acids Res.* **2023**, *51*, 2529–2573.
- [4] *Combination Therapy Against Multidrug Resistance*, (Eds.: M. Wani, A. Ahmad), Academic Press, **2020**.
- [5] V. Elez, WO2004054657A1, **2003**.
- [6] X. Zhang, W. Niu, M. Mu, S. Hu, C. Niu, *J. Exp. Clin. Cancer Res.* **2020**, *22*, 196.
- [7] R. R. Banala, S. K. Vemuri, G. H. Dar, V. Palanisamy, M. Penkulinti, M. V. Surekha, A. V. G. Reddy, M. R. Nalam, G. P. V. Subbai-ah, *Spine J.* **2019**, *19*, 896–904.
- [8] M. L. Uribe, I. Marrocco, Y. Yarden, *Cancers* **2021**, *13*, 2748.
- [9] C. V. Dang, L. M. S. Resar, E. Emison, S. Kim, Q. Li, J. E. Prescott, D. Wonsley, K. Zeller, *Exp. Cell Res.* **1999**, *253*, 63–77.
- [10] V. Llombart, M. R. Mansour, *EBioMedicine* **2022**, *75*, 103756.
- [11] G. Donati, B. Amati, *Mol. Oncol.* **2022**, *16*, 3828–3854.
- [12] Z. Tang, C. Li, B. Kang, G. Gao, C. Li, Z. Zhang, *Nucleic Acids Res.* **2017**, *45*, 98–102.
- [13] W. Park, A. Chawla, E. M. O'Reilly, *Jama* **2021**, *326*, 851–862.
- [14] A. K. Witkiewicz, E. A. McMillan, U. Balaji, G. Baek, W. C. Lin, J. Mansour, M. Mollaei, K. U. Wagner, P. Koduru, A. Yopp, M. A. Choti, C. J. Yeo, P. McCue, *Nat. Commun.* **2015**, *6*, 6744.
- [15] H. Lin, C. Hu, S. Zheng, X. Zhang, R. Chen, Q. Zhou, *Aging* **2021**, *13*, 12493–12513.
- [16] D. Kaniowski, K. Ebenryter-Olbińska, K. Kulik, S. Janczak, A. Maciaszek, K. Bednarska-Szczepaniak, B. Nawrot, Z. J. Lesnikowski, *Nanoscale* **2020**, *12*, 103–114.
- [17] D. Kaniowski, K. Ebenryter-Olbińska, K. Kulik, J. Suwara, W. Cypryk, A. Jakóbiak-Kolon, Z. J. Lesnikowski, B. Nawrot, *Int. J. Mol. Sci.* **2021**, *22*, 4863.
- [18] A. R. Nourazarian, A. G. Najar, S. Farajnia, A. Y. Khosroushahi, R. Pashaei-Asl, Y. Omid, *Asian Pac. J. Cancer P.* **2012**, *13*, 4751–4756.
- [19] A. K. Petch, M. Sohail, M. D. Hughes, I. Benter, J. Darling, E. M. Southern, S. Akhtar, *Biochem. Pharmacol.* **2003**, *66*, 819–830.
- [20] M. R. Bennett, S. Anglin, J. R. McEwan, R. Jagoe, A. C. Newby, G. I. Evan, *J. Clin. Invest.* **1994**, *93*, 820–828.
- [21] T. Goto, K. Ohta, T. Suzuki, S. Ohta, Y. Endo, *Bioorg. Med. Chem.* **2005**, *13*, 6414–6424.
- [22] H. Nakamura, K. Aoyagi, Y. Yamamoto, *J. Am. Chem. Soc.* **1998**, *120*, 1167–1171.
- [23] S. Janczak, A. Olejniczak, S. Balabańska, M. K. Chmielewski, M. Lupu, C. Viñas, Z. J. Lesnikowski, *Chem. Eur. J.* **2015**, *21*, 15118–15122.
- [24] T. Brown, D. J. S. Brown in *Oligonucleotides and analogues. A Practical Approach*, (Ed. F. Eckstein), IRL Press, Oxford, **1991**, pp. 1–24.
- [25] Z. J. Leśnikowski, *J. Med. Chem.* **2016**, *59*, 7738–7758.
- [26] J. S. Carroll, A. Swarbrick, E. A. Musgrove, R. L. Sutherland, *Cancer Res.* **2002**, *62*, 3126–3131.
- [27] S. Ochoa, W. T. Milam, *Molecules* **2020**, *25*, 4659.
- [28] J. A. McDowell, D. H. Turner, *Biochemistry* **1996**, *35*, 14077–89.
- [29] E. A. Lesnik, S. M. Freier, *Biochemistry* **1995**, *34*, 10807–10815.
- [30] N. Sugimoto, N. Shu-Chi, M. Katoh, A. Matsumura, H. Nakamura, T. Ohmichi, M. Yoneyama, M. Sasaki, *Biochemistry* **1995**, *34*, 11211–11216.
- [31] C. A. Stein, *J. Clin. Invest.* **2001**, *108*, 641–644.
- [32] N. Iwamoto, D. C. D. Butler, N. Svrzikapa, S. Mohapatra, I. Zlatev, D. W. Y. Sah Meena, S. M. Standley, G. Lu, L. H. Apponi, M. Frank-Kamenetsky, J. J. Zhang, C. Vargeese, G. L. Verdine, *Nat. Biotechnol.* **2017**, *35*, 845–851.
- [33] Z. J. Lesnikowski, *Nucleos. Nucleot.* **1992**, *11*, 1621–1638.
- [34] Z. J. Lesnikowski, *Bioorg. Chem.* **1993**, *21*, 127–155.
- [35] H. Jahns, N. Taneja, J. L. S. Willoughby, M. Akabane-Nakata, C. R. Brown, T. Nguyen, A. Bisbe, S. Matsuda, M. Hettlinger, R. M. Manoharan, K. G. Rajeev, M. A. Maier, I. Zlatev, K. Charisse, M. Egli, M. Manoharan, *Nucleic Acids Res.* **2022**, *50*, 1221–1240.
- [36] H. Takakusa, N. Iwazaki, M. Nishikawa, T. Tokuyuki Yoshida, S. Obika, T. Inoue, *Nucleic Acid Ther.* **2023**, *33*, 83–94.
- [37] Z. J. Lesnikowski, G. Fulcrand, R. M. Lloyd, A. Juodawlkis, R. F. Schinazi, *Biochemistry* **1996**, *35*, 5741–5746.
- [38] A. Szala, S. Sawicki, A. S. Swierzko, J. Szemraj, M. Sniadecki, M. Michalski, A. Kaluzynski, J. Lukasiewicz, A. Maciejewska, D. Wydra, D. C. Kilpatrick, M. Matsushita, M. Cedzynski, *Cancer Immunol. Immunother.* **2013**, *62*, 1411–1419.
- [39] A. S. Swierzko, K. Florczak, M. Cedzyński, J. Szemraj, D. Wydra, L. Bak-Romaniszyn, J. Emerich, Z. Sułowska, *Cancer Immunol. Immunother.* **2007**, *56*, 959–971.
- [40] T. M. Goszczyński, K. Fink, K. Kowalski, Z. J. Leśnikowski, J. Boratyński, *Sci. Rep.* **2017**, *7*, 9800.
- [41] D. Kaniowski, K. Kulik, J. Suwara, K. Ebenryter-Olbińska, B. Nawrot, *Int. J. Mol. Sci.* **2022**, *23*, 12190.
- [42] J. Schindelin, I. Arganda-Carreras, E. Frise, V. Kaynig, M. Longair, T. Pietzsch, S. Preibisch, C. Rueden, S. Saalfeld, B. Schmid, J.-Y. Tinevez, D. J. White, V. Hartenstein, K. Eliceiri, P. Tomancak, A. Cardona, *Nat. Methods* **2019**, *9*, 676–682.
- [43] L. McAlary, J. A. Aquilina, J. J. Yerbury, *Front. Neurol. Neurosci.* **2016**, *10*, 499.
- [44] T. Mosmann, *J. Immunol. Methods.* **1983**, *65*, 55–63.
- [45] G. Gajek, B. Marciniak, J. Lewkowski, R. Kontek, *Molecules* **2020**, *25*, 658.
- [46] K. Bednarska-Szczepaniak, E. Przelazły, K. D. Kania, M. Szwed, M. Litecka, B. Grüner, Z. J. Leśnikowski, *Cancers* **2021**, *13*, 3855.

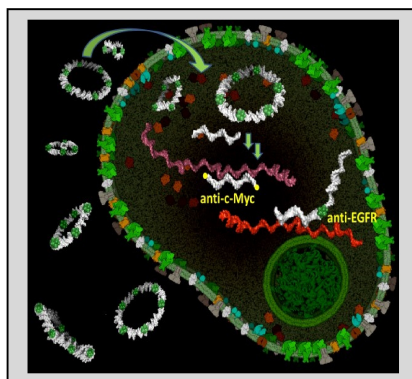
Manuscript received: October 25, 2023

Accepted manuscript online: January 12, 2024

Version of record online: ■ ■ ■ ■ ■

## RESEARCH ARTICLE

A versatile method for the automated synthesis of composites containing DNA-oligonucleotides and boron cluster scaffolds and their assembly into functional nanoparticles is described. The torus-like nanostructures carry antisense oligonucleotides that target two different oncogenes and act as dual-action agents silencing two oncogenes EGFR and c-Myc simultaneously. The system can be readily adapted to target other biological components.



*Dr. K. Bednarska-Szczepaniak, Dr. K. Ebenryter-Olbińska, Dr. G. Gajek, K. Śmiałkowski, Dr. J. Suwara, L. Fiedorowicz, Prof. Z. Leśniowski\**

1 – 11

**Synthesis of DNA-boron cluster composites and assembly into functional nanoparticles with dual, anti-EGFR, and anti-c-MYC oncogene silencing activity**

